Korean J. Chem. Eng., 38(7), 1499-1509 (2021)
DOI: 10.1007/s11814-021-0801-9

pISSN: 0256-1115
eISSN: 1975-7220

Numerical desirability function for adsorption of methylene blue dye by sulfonated pomegranate peel biochar: Modeling, kinetic, isotherm, thermodynamic, and mechanism study

Ali H. Jawad*,†, Ahmed Saud Abdulhameed, M. A. K. M. Hanafiah***, Zeid A. ALOthman****, Mohammad Rizwan Khan****, and S. N. Surip***

*Faculty of Applied Sciences, Universiti Teknologi MARA, 40450 Shah Alam, Selangor, Malaysia
**Department of Medical Instrumentation Engineering, Al-Mansour University College, Baghdad, Iraq
***Faculty of Applied Sciences, Universiti Teknologi MARA, 26400 Jengka, Pahang, Malaysia
****Advanced Materials Research Chair, Chemistry Department, College of Science, King Saud University, Riyadh 11451, Saudi Arabia
(*Received 24 October 2020 • Revised 4 April 2021 • Accepted 11 April 2021*)

Abstract−Sulfonated pomegranate (*Punica granatum*) peel biochar (SPPBC) was developed *via* thermal activation with sulfuric acid (H_2SO_4) to act as a promising biochar material for the adsorptive removal of toxic cationic dye namely methylene blue (MB) dye from contaminated water. A Box-Behnken design (BBD) and numerical desirability function were adopted to optimize the input adsorption variables (SPPBC dosage, temperature, pH, and contact time). The maximum removal of the MB dye can be accomplished by simultaneous significant interaction between SPPBC dosage with solution pH, SPPBC dosage with time, SPPBC dosage with temperature, solution pH with time, and time with temperature. The numerical desirability function identified the highest MB dye removal (93.9%) can be achieved at the following optimum numerical adsorption conditions: SPPBC dosage 0.18 g, temperature 49 °C, pH 9.7, and time 4.3 h. Equilibrium data were well fitted to the Temkin and Langmuir isotherm models. The maximum recorded adsorption capacity of SPPBC for MB dye adsorption by using Langmuir isotherm model was 161.9 mg/g. This research work reveals the possibility of converting lignocellulose pomegranate peel into a renewable and environment-friendly biochar *via* a relatively fast acid-activation process with the great potential to be promising adsorbent for removal of MB dye.

Keywords: Adsorption, Biochar, Box-Behnken Design, Methylene Blue, Pomegranate Peel, Sulfuric Acid

INTRODUCTION

The discharged synthetic organic dyes into water bodies have been known to be one of the major causes of changes in odor, color, taste, pH, and chemical oxygen demand (COD) [1]. Methylene blue dye (MB) is commonly released from textiles, plastics, food, cosmetics, leather, and pharmaceuticals industries [2]. MB dye can cause serious health problems such as nausea, improper breathing, vomiting, necrosis, gastritis, nausea symptoms diarrhea, and mental confusion [3]. Different treatment methods that have been reported for removing of synthetic dyes from wastewaters include photocatalysis [4], biological treatment [5], adsorption [6], and membrane filtration [7]. Among various treatment methods, adsorption is an easy and effective method for removing synthetic dyes because of its simplicity in design, reusability of adsorbent, selectivity towards water contaminants, and less operation cost [8].

Activated carbon (AC) is the most common adsorbent used to remove various water/air pollutants in industrial processes, such as drinking water purification, air purification, and wastewater treatment facilities [9]. However, the preparation of AC usually involves high energy and cost consequences [10]. Moreover, unlimited non-renewable materials such as petroleum coke, lignite, and coal have been used as non-sustainable precursors for developing AC [11]. Therefore, research efforts have been shifted to find alternative renewable and sustainable precursors and cost-effective preparation method for producing carbon-based adsorbent materials. Biochar (BC) is a solid carbonaceous material that presents itself as a promising alternative to commercial AC in various environmental technologies to remove pollutants from wastewater [12]. Production of BC always involves several desirable outcomes, such as low operation cost, mild operation conditions, moderate activation temperature, availability of plenty functional groups on its surface, economic, and environmental benefits [12].

Application of BC in industrial treatment facilities has some drawbacks due to BC's low surface area and poor adsorption affinity towards some organic pollutants or heavy metals [13]. The adsorptive property of carbon-based adsorbents mainly depends on surface area and surface group functionality or both. Several activation methods such as chemical surface modification (hydrothermal carbonization), high pyrolysis temperature, and gasification have been applied to modify crude precursors for preparation of high surface area AC [14]. Although pyrolysis method may improve the

†To whom correspondence should be addressed.
E-mail: ali288@uitm.edu.my, ahjm72@gmail.com

surface area property in terms of pore structure and specific surface area, it leads to the decrease of AC surface functional groups and consumes a high amount of electrical energy [15]. Another successful alternative is the adsorbent surface functionalization method, which offers various desirable adsorption active sites on the adsorbent surface for better affinity toward targeted pollutants [16].

In general, functionalized carbon-based materials have received significant attention due to many desirable properties, such as high selectivity of adsorbents towards a specific class of water contaminants, cost-effective preparation method, and high yield of products. The sulfonation process is a critical step of chemical activation, which produces acid-rich sites on carbon-based materials [17-19]. In this regard, various sulfonation approaches have been reported, which include H_2SO_4 acid [20], 4-benzenediazonium sulfonate [21], sodium dodecylbenzene sulfonate (SDBS), and sodium dodecyl sulfate (SDS) [22]. Among these chemical activators, H_2SO_4 acid is one of the most efficient chemical activators for biomass materials due to its exceptional features, such as introducing plenty of active sites (e.g. -SO_3H groups), cost-effectiveness, relatively low activation temperature required to achieve the activation process, super oxidation power, and the activation process can be accomplished in a single step [23]. Moreover, sulfonated biochar has been successfully applied in various demanded applications, such as catalytic reaction [17], biofuel production [24], and promising adsorbent for various water contaminants [25-27].

Thus, this work aims to use pomegranate peel (PP) as a low-cost precursor for producing sulfonated pomegranate peel biochar (SPPBC) as a functionalized and selective adsorbent *via* thermal activation with H_2SO_4 acid. The adsorptive property of acidic SPPBC adsorbent was evaluated to remove cationic MB dye using the Response Surface Methodology-Box-Behnken design (RSM-BBD). The RSM-BBD was used to optimize critical parameters such as SPPBC dosage, solution pH, time, and temperature. The rate of uptake or kinetics, thermodynamics, and mechanism of MB dye by SPPBC will be discussed.

MATERIALS AND METHODS

1. Materials and Chemicals

The pomegranate peel (PP) was obtained from a market located in Shah Alam, Malaysia. MB dye (99% purity, λ_{max}=661 nm) and concentrated (97% w/v) sulfuric acid (H_2SO_4) were purchased from the R&M Chemicals, Malaysia. Ultra-pure water was used in the preparation of reagents and working solutions.

2. Synthesis of SPPBC

PP was repeatedly rinsed with distilled water, dried in an oven at 80 °C for 24 h, and ground and sieved to obtain the particle size of 250-500 μm. The activation process was done by mixing 1 g of PP powder with 1 mL of H_2SO_4 solution based on published procedure [19,23]. The blend was left in an oven at 110 °C for 24 h. The final yield of SPPBC was washed with boiled water until neutral solution pH reached. Then, SPPBC was dried in an oven for 24 h at 100 °C, and finally it was ground to obtain a uniform particle size of 250 μm for additional applications.

3. SPPBC Characterization

The specific surface area of SPPBC was obtained from the Micromeritics ASAP 2060 surface analyzer by the application of the Brunauer-Emmett-Teller (BET) equation. The scanning electron microscopy images were characterized using a Zeiss Supra 40 VP scanning electron microscope (SEM). The crystallinity and amorphous nature of SPPBC were examined by X-ray diffraction (XRD, X'Pert PRO, PAnalytical) machine with a 2θ range from 0 to 80° using Cu-K_α as the radiation source. The identification of the functional groups was done by Fourier transform infrared (FTIR) spectrophotometer (Perkin-Elmer, Spectrum RX I). The elemental composition of SPPBC was analyzed using the CHNS-O Analyzer (Flash 2000, Thermo-scientific).

4. Experimental Design

The BBD based on RSM (Stat-Ease Design-Expert software, version 13.0) was utilized for the purpose of optimizing the input key parameters with their ranges as given in Table 1. The MB dye removal prediction was calculated based on the second-order quadratic model, given by Eq. (1) [28].

$$Y = \beta_0 + \sum \beta_i X_i + \sum \beta_{ii} X_i^2 + \sum\sum \beta_{ij} X_i X_j \quad (1)$$

Y is the expected response (MB dye removal (%)); X_i and X_j are independent variables; $-\beta_0$, β_i, β_{ii} and β_{ij} are constant, coefficients of linear, quadratic, and interaction coefficient, respectively. Table 2 gives the obtained results of MB dye removal (%) based on BBD model. An accurate amount (g) of SPPBC was weighed and added to 100 mg/L MB dye solution (100 mL) before being shaken in a thermostat water bath shaker. The MB dye concentration was measured using a UV-Visible spectrophotometer (HACH, model DR 3900) at λ_{max} 661 nm. The percentage of MB dye removal (DR %) was calculated using Eq. (2):

$$DR\ \% = \frac{(C_o - C_e)}{C_o} \times 100\% \quad (2)$$

where C_o (mg/L) is MB concentration at initial, whereas C_e (mg/L) is MB concentration at final.

5. Adsorption of MB Dye by SPPBC

MB dye adsorption experiments were studied in batch mode based on the numerical desirability function. The best optimized adsorption conditions were determined to be SPPBC dosage of

Table 1. Codes and actual variables and their levels in BBD

Codes	Variables	Level 1 (−1)	Level 2 (0)	Level 3 (+1)
A	SPPBC dosage (g)	0.05	0.15	0.25
B	pH	3	6.5	10
C	Temperature (°C)	30	40	50
D	Time (h)	2	4	6

Table 2. The 4-varibles BBD matrix and experimental data for MB removal efficiency

Run	A: SPPBC dosage (g)	B: pH	C: Temp. (°C)	D: Time (h)	MB removal
1	0.05	3	40	4	7.5
2	0.25	3	40	4	50.2
3	0.05	10	40	4	10.4
4	0.25	10	40	4	89.6
5	0.15	6.5	30	2	10.5
6	0.15	6.5	50	2	30.1
7	0.15	6.5	30	6	15.2
8	0.15	6.5	50	6	88.4
9	0.05	6.5	40	2	5.9
10	0.25	6.5	40	2	32.9
11	0.05	6.5	40	6	6.8
12	0.25	6.5	40	6	89.2
13	0.15	3	30	4	13.2
14	0.15	10	30	4	16.1
15	0.15	3	50	4	45.2
16	0.15	10	50	4	87.9
17	0.05	6.5	30	4	6.6
18	0.25	6.5	30	4	29.8
19	0.05	6.5	50	4	7.4
20	0.25	6.5	50	4	92.8
21	0.15	3	40	2	14.7
22	0.15	10	40	2	23.7
23	0.15	3	40	6	27.6
24	0.15	10	40	6	47.8
25	0.15	6.5	40	4	26.5
26	0.15	6.5	40	4	21.1
27	0.15	6.5	40	4	29.9
28	0.15	6.5	40	4	24.7
29	0.15	6.5	40	4	23.2

0.18 g, pH of 9.7, temperature of 49 °C, and contact time of 3.4 h, which gave 93.9% of MB dye removal. Therefore, all adsorption experiments were out at these optimal conditions. The initial MB dye concentrations were varied from 10 to 300 mg/L, while the contact times were varied from 0 to 25 h. At equilibrium time, the adsorption capacity of SPPBC (q_e (mg/g)) was estimated using Eq. (3):

$$q_e = \frac{(C_o - C_e)V}{W} \quad (3)$$

where V (L) is the volume of MB solution, W (g) is the quantity of the adsorbent.

RESULTS AND DISCUSSION

1. SPPBC Characterization

The results of CHNS analysis are given in Table 3. SPPBC elemental composition was found as follows: C (45.31%), H (3.74%), N (0.78%), S (0.23%) and O (49.92% by difference). The detected S can be assigned to the sulfonated SPPBC with -SO_3H groups in its structure, which is a highly demanded acidic functional group for capturing cationic dye molecules. As shown in Table 3, the surface area of SPPBC was found to be quite low (1.01 m^2/g). Meanwhile, the mean pore diameter was 181.9 nm, an indication of a macroporous structure (mean pore diameter >50 nm) based on IUPAC classification [29].

Table 3. The elemental analysis and textural properties of SPPBC

Elemental analysis (wt%)	SPPBC
C	45.31
H	3.74
N	0.78
S	0.23
O (by difference)	49.92
Surface property	**SPPBC**
Vm (cm^3/g)	0.00011
Total pore volume (cm^3/g)	0.00023
BET surface area (m^2/g)	1.01
Mean pore diameter (nm)	181.9

The XRD pattern of the SPPBC (Fig. 1) demonstrates major broad peaks (2θ=23° and 44°) that correspond to the (002) and

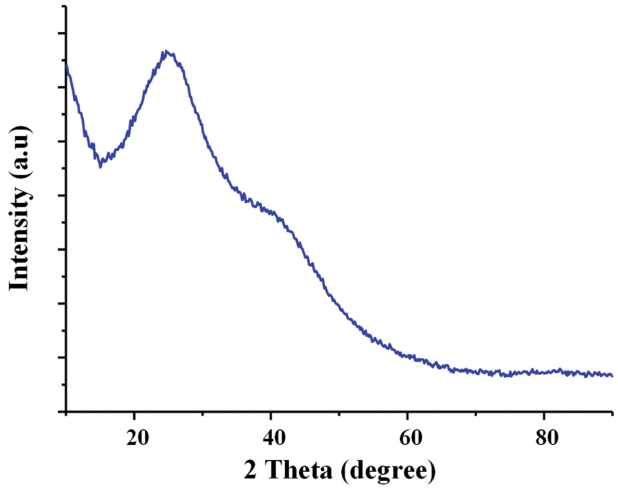

Fig. 1. XRD pattern of SPPBC.

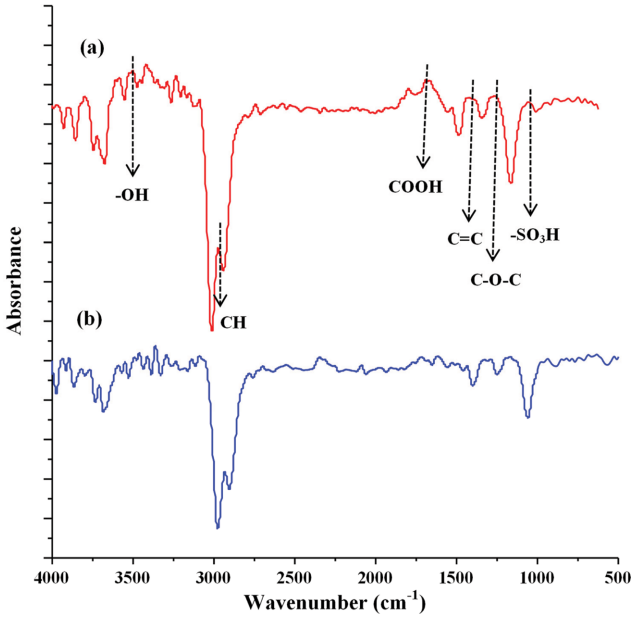

Fig. 2. FTIR spectra of (a) SPPBC, and (b) SPPBC after adsorption of MB dye.

(100) phases, respectively. These broad peaks can be assigned to the graphite crystallites signature and signifies the amorphous nature of SPPBC [30].

The FTIR spectra of SPPBC (before and after MB dye adsorption) are shown in Fig. 2. The characteristic IR bands of SPPBC (Fig. 2(a)) are assigned as follows: 3,500 to 3,350 cm^{-1}, 2,900 cm^{-1}, 1,720 cm^{-1}, 1,540 cm^{-1}, 1,200 cm^{-1}, and 1,090 cm^{-1}, which represent the hydroxyl (-OH), alkyl (C-H), carboxyl (-COOH), alkene (C=C), ether (C-O-C), and sulfonic (-SO_3H) groups, respectively [17]. This result illustrates that the sulfonation process of the PP could provide different acidic functional groups such as -COOH and -SO_3H on the SPPBC surface. The FTIR spectrum of SPPBC after MB dye adsorption (Fig. 2(b)) did not show much difference from the SPPBC spectrum before adsorption. Except, some slight

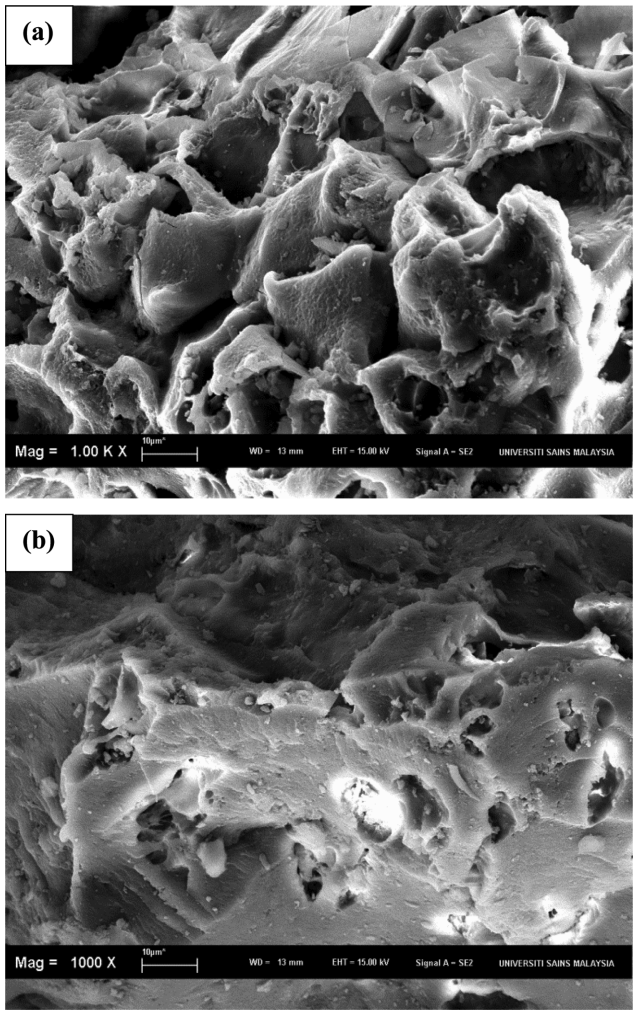

Fig. 3. SEM images of (a) SPPBC, and (b) SPPBC after adsorption of MB dye.

shifts in IR peaks' locations can be detected, which might provide evidence that the acidic functional groups are responsible for capturing the MB cationic dye molecules.

The surface morphology of SPPBC was explored before and after MB dye adsorption onto its surface with SEM as shown in Fig. 3. As shown in Fig. 3(a), SPPBC has irregular and wavy surface with numerous pores and crevices and could be considered heterogeneous. The porous and rough structure of the SPPBC favored the MB dye adsorption. On the other hand, after MB dye adsorption, the SPPBC surface became more compact with attenuated porosity, as shown in Fig. 3(b).

2. BBD Model Analysis

Table 4 shows the analysis of variance (ANOVA) results, which was used to validate the statistical analysis. The F-value of the MB removal model is 36.02 (p-value<0.0001), which suggested that the BBD model was statistically significant [31]. Moreover, the high correlation coefficient (R^2=0.97) indicated the high compatibility between expected and experimental MB values [32]. The BBD terms are considered statistically significant when the p-value<0.05 under selected conditions, as shown in Table 4. The relationship between

Table 4. Analysis of variance (ANOVA) for the removal efficiency of MB

Source	Sum of squares	df	Mean square	F-value	p-Value	Remark
Model	22,316.87	14	1,594.06	36.02	<0.0001	S
A-Dose	9,627.67	1	9,627.67	217.56	<0.0001	S
B-pH	1,142.70	1	1,142.70	25.82	0.0002	S
C-Temp.	5,650.68	1	5,650.68	127.69	<0.0001	S
D-Time	2,059.32	1	2,059.32	46.54	<0.0001	S
AB	333.06	1	333.06	7.53	0.0158	S
AC	967.21	1	967.21	21.86	0.0004	S
AD	767.29	1	767.29	17.34	0.0010	S
BC	396.01	1	396.01	8.95	0.0097	S
BD	31.36	1	31.36	0.7087	0.4140	NS
CD	718.24	1	718.24	16.23	0.0012	S
A^2	210.87	1	210.87	4.77	0.0466	S
B^2	257.58	1	257.58	5.82	0.0301	S
C^2	361.39	1	361.39	8.17	0.0127	S
D^2	8.79	1	8.79	0.1987	0.6626	NS
Residual	619.54	14	44.25			
Lack of fit	574.77	10	57.48	5.14	0.0644	NS
Pure error	44.77	4	11.19			
Cor total	22,936.40	28				

S: Significant; NS: Not significant; R^2=0.97; Adjusted R^2=0.95

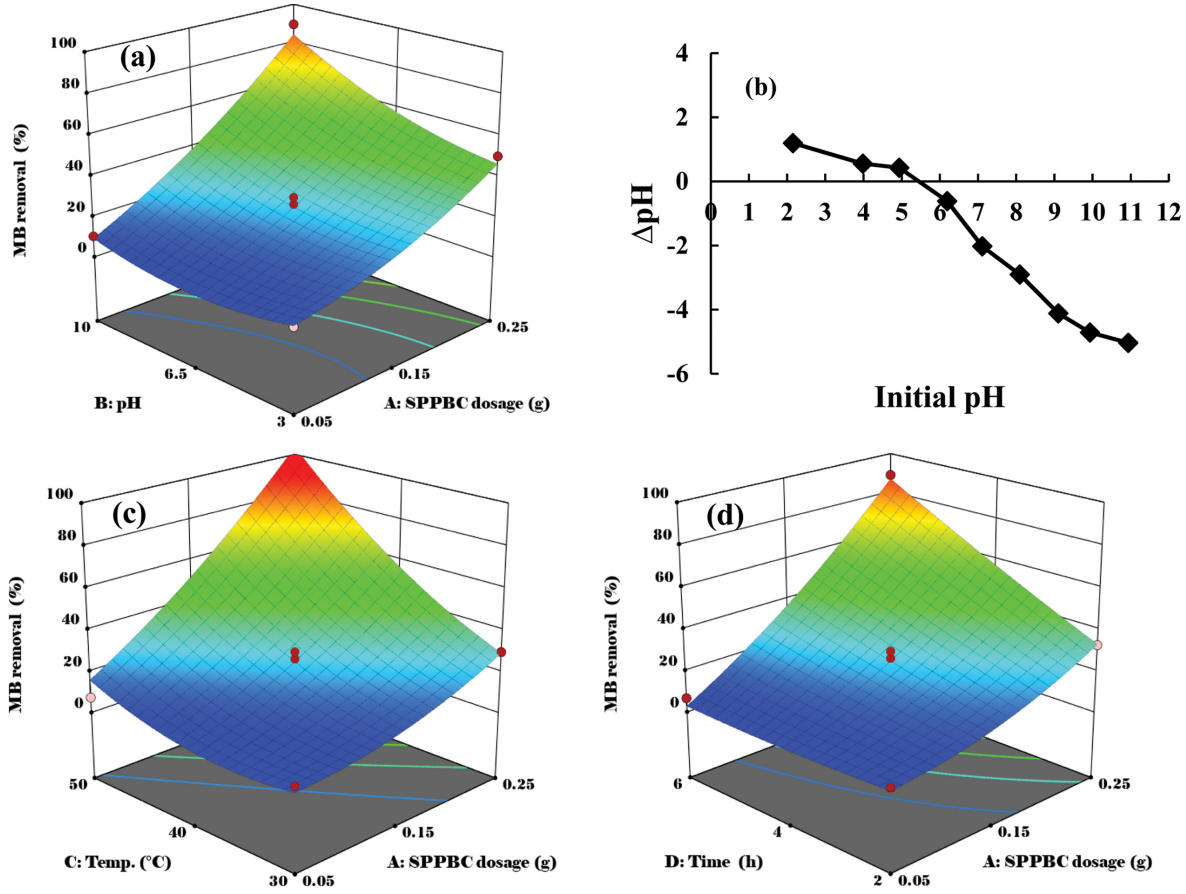

Fig. 4. (a) 3D response surface plot of MB removal efficiency showing interaction between SPPBC dosage and pH, and (b) pH_{PZC} of SPPBC, (c) 3D response surface plot of MB removal efficiency showing interaction between SPPBC dosage and temperature and (d) 3D response surface plot of MB removal efficiency showing interaction between SPPBC dosage and time.

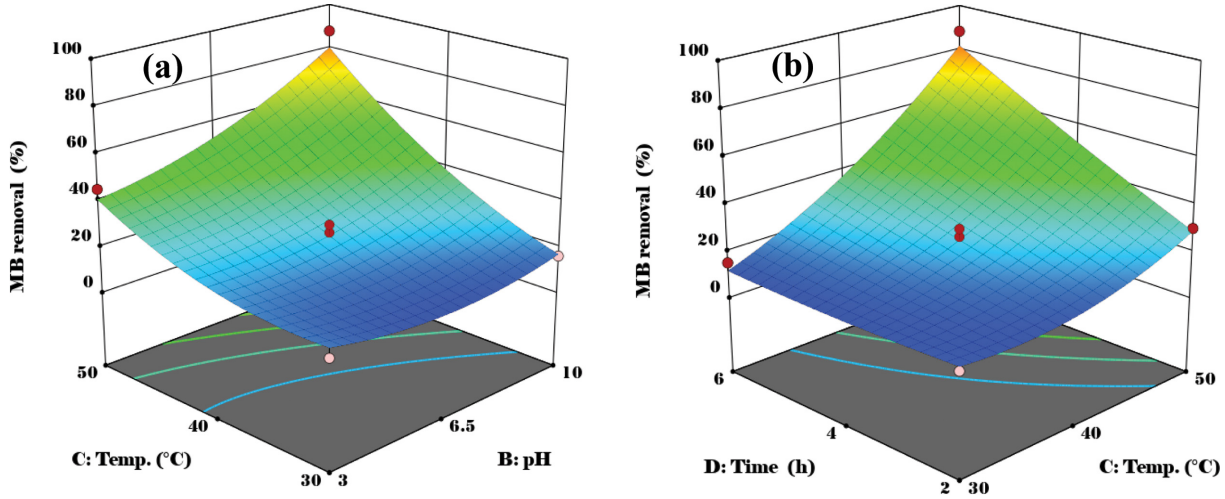

Fig. 5. (a) 3D response surface plot of MB removal efficiency showing interaction between pH and temperature, and (b) 3D response surface plot of MB removal efficiency showing interaction between temperature and time.

tested variables and the response can be expressed using a second-order polynomial (Eq. (4)):

$$\text{MB removal (\%)}=25.08+28.33A+9.76B+21.70C+13.10D+9.13AB+15.55AC+13.85AD+9.95BC+13.40CD+5.70A^2+6.30D^2+7.46C^2 \quad (4)$$

A non-significant lack of fit (LOF) related to the pure error indicates an excellent response to the experimental results [33]. Thus, it can be deduced that BBD model was suitable to expect the removal of MB dye on the surface of SPPBC within the range of the studied parameters.

3. Significant Interactions of Parameters

The p-value of 0.0158 indicated that the relationship between SPPBC dosage and pH, while keeping the temperature and contact time constant, was statistically significant (Table 4). Fig. 4(a) presents the 3D surface plot of the combined effect of SPPBC dosage and pH. The MB dye removal (%) was found to increase by increasing the solution pH from 3 to 10. In Fig. 4(b), the pH of the point of zero charges (pH_{pzc}) of the SPPBC was found to be 5.4. Therefore, the SPPBC surface would take a more positive charge if the pH of the MB dye solution was less than pH_{pzc}. By contrast, the SPPBC surface charge would carry a more negative charge at pH 10, which favored the MB dye adsorption. As a result, the electrostatic attractions would occur between negatively charged SPPBC surface and positively charged MB dye, denoted in Eq. (5):

$$SPPBC\text{-}SO_3^- + MB^+ \leftrightarrow SPPBC\text{-}SO_3^- \ldots {}^+MB \quad (5)$$

The interaction between SPPBC dosage with temperature and time was statistically significant (p-value=0.0004 for dosage×temperature, and p-value=0.0010 for dosage×time), as shown by the 3D response surfaces plots (Fig. 4). Fig. 4(c) shows that the MB dye removal increased from 5.9% to 92.8% as SPPBC dosage increased from 0.05 to 0.25 g. This increasing trend could be explained in terms of the higher number of active adsorption sites as the SPPBC surface area increased. As shown in Fig. 4(d), a longer contact time (6 h) was more efficient in removing MB dye from the solutions, possibly due to the adequate time to overcome the internal diffusion process.

The interaction between temperature with solution pH and contact time was also statistically significant (p-value=0.0097 for temperature×pH, and p-value=0.0012 for temperature×time). As shown by the 3D response surfaces plots (Fig. 5). In general, Fig. 5(a) and 5(b) shows that MB dye removal was more effective at a higher temperature (50 °C) than at lower temperatures, indicating an endothermic reaction [34]. The dye removal (%) increased with rising temperatures and solution pH up to 50 °C and 10, respectively (Fig. 5(a)), indicating that the ionization process of dye molecules became more pronounced at a higher temperature, leading to an enhanced adsorption process. Moreover, increasing the temperature would facilitate more diffusion of adsorbate molecules into the adsorbent interspaces structure [35].

4. Optimization using the Desirability Functions

Derringer's desirability function or known as desirability function is a multi-response optimization method developed by Derringer and Suich (1980) [6]. In this method, each individual response first converts into the individual desirability (di) within a numerical range of 0-1. The desirability value of 1 means the desirable value of response was attended. In contrast, the desirability value of 0 means the value of response goes over the required acceptable threshold value [8]. Eq. (6) can be utilized to calculate the overall desirability function.

$$D=(d_1\times d_2\times \ldots \times d_n)^{\frac{1}{n}}=(\Pi_{i=1}^{n} d_1)^{\frac{1}{n}} \quad (6)$$

In Eq. (6), D presents the overall desirability, di shows individual desirability, and n reflects the total number of responses [6,8]. The main target is to determine a point in which the desirability has a maximum value. Thus, a desirability function is an established method used to find the simultaneous optimization of process variables (A: SPPBC dosage, B: pH, C: temperature, and D: time) that achieves optimum performance level for the response (MB removal %), and the thorough procedure had been previously described [36]. The numerical optimization of the software demon-

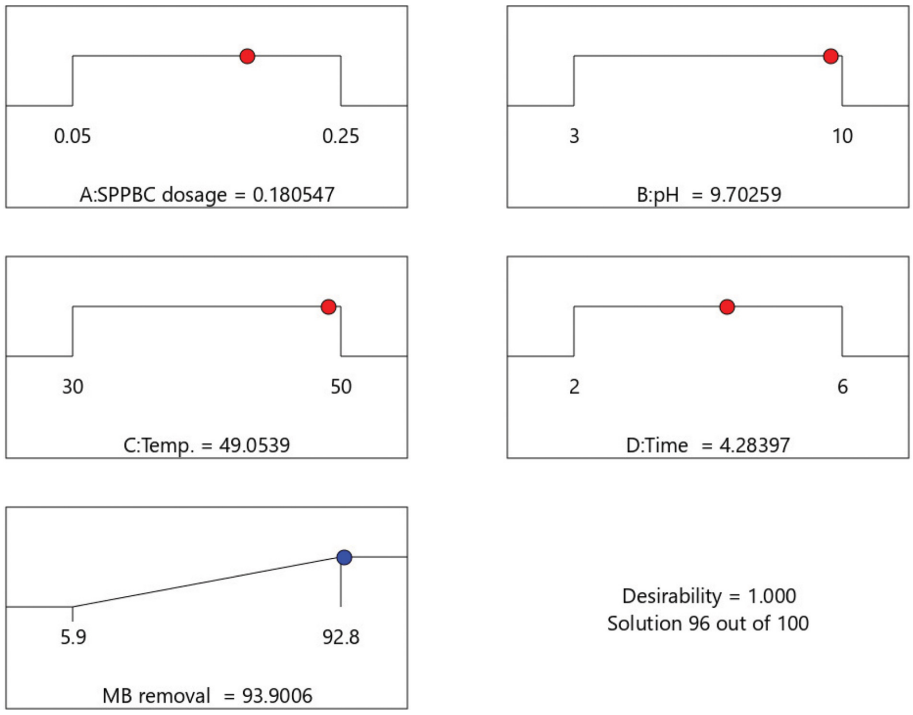

Fig. 6. Desirability ramps for the optimization of important adsorption input parameters for MB dye removal (%) by SPPBC.

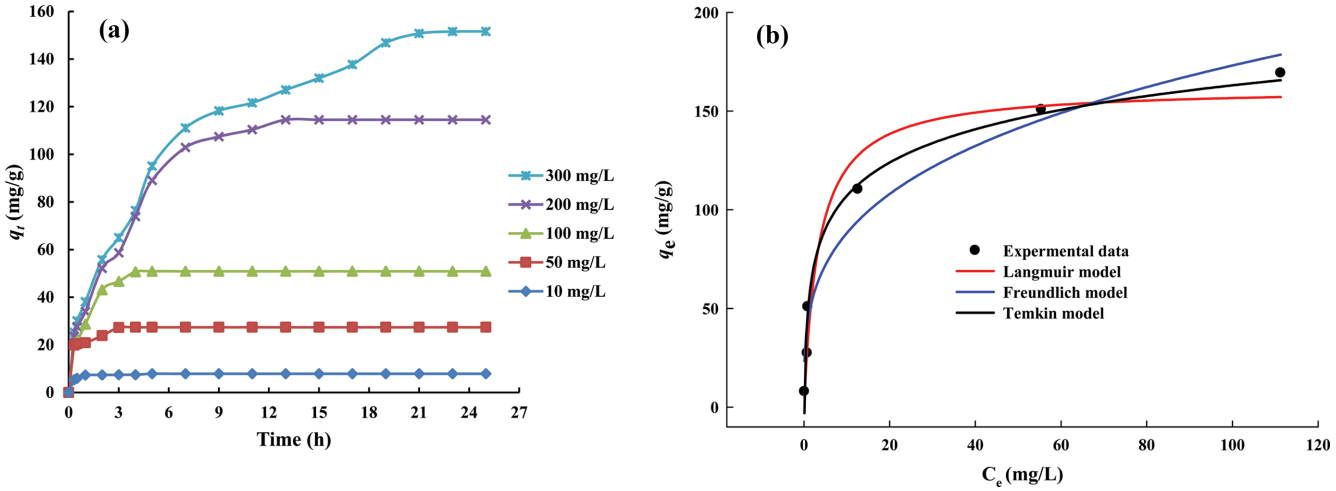

Fig. 7. (a) Effect of the contact time on MB adsorption at different initial concentrations and (b) adsorption isotherms of MB by SPPBC (dosage=0.18 g, pH of solution=9.7, temperature=49 °C, agitation speed=100 strokes and volume of solution=100 mL).

strated the optimal removal of MB was obtained at SPPBC dosage of 0.18 g, solution pH of 9.7, temperature of 49 °C, and time of 4.3 h; at these operation conditions the MB removal is 93.9% with desirability value of 1 as shown in Fig. 6. The validity of this prediction was checked by duplicate confirmatory experiments under the optimized parameters. Overall, the results obtained from experimental data were in a good agreement with data obtained from numerical optimization using desirability functions. This indicated that the BBD model with desirability functions can be effectively used for optimizing the experimental conditions of MB adsorption by SPPBC. Therefore, the optimal experimental conditions of MB adsorption were applied in the subsequent works.

5. Kinetic Study

The effect of contact time on MB dye adsorption at five different concentrations (10, 50, 100, 200, and 300 mg/L) is shown in Fig. 7(a). Other optimal parameters, such as SPPBC dosage, pH, and temperature, were kept constant. The amount of MB dye adsorbed increased from 7.9 to 151.6 mg/g with the increase in the MB dye concentration from 10 to 300 mg/L. As the concentration increased, the diffusion of MB dye into the pores would be accelerated. Therefore, a much higher driving force would outdo the mass transfer resistance between SPPBC surface and adsorbate molecules [37]. Two non-linear equations of the pseudo-first order (PFO) [38] and pseudo-second order (PSO) [39] were applied to

Table 5. PFO and PSO kinetic parameters for MB adsorption by SPPBC at 0.18 g dosage, solution pH 9.7, and temperature 49 °C

Concentration (mg/L)	q_e (mg/g)	PFO				PSO			
		q_e (mg/g)	k_1 (1/h)	R^2	SSE	q_e (mg/g)	k_2 (g/mg h)	R^2	SSE
10	7.9	7.8	3.236	0.99	0.67	8.0	1.220	0.98	0.27
50	27.4	26.9	3.113	0.94	42.7	27.7	0.209	0.98	15.5
100	50.9	50.7	1.024	0.98	60.7	53.8	0.030	0.98	76.7
200	114.5	115.1	0.293	0.98	455.5	132.4	0.002	0.98	493.6
300	151.6	146.0	0.202	0.93	514.5	176.9	0.001	0.99	571.3

determine the adsorption kinetics parameters. Both equations are given by Eqs. (7) and (8), respectively:

$$q_t = q_e(1-\exp^{-k_1 t}) \quad (7)$$

$$q_t = \frac{q_e^2 k_2 t}{1+q_e k_2 t} \quad (8)$$

where, q_t, q_e, k_1 and k_2 represent the amount (mg/g) of MB dye adsorbed at time t (min), at equilibrium time, the PFO rate constant (1/min), and the PSO rate constant (g/mg min), respectively. Moreover, to identify the best fitting model for the data, the correlation coefficient (R^2) and the sum of square errors (SSE) were used to analyze the differences between the experimental data and the theoretical data obtained from the models. The sum of square errors (SSE) was calculated according to the mathematical formula expressed in Eq. (9):

$$SSE = \sum_{1}^{n}(q_{exp} - q_{cal})^2 \quad (9)$$

Table 5 summarizes the important kinetic parameters, and it was found that the R^2 values of PFO and PSO are close to each other. Therefore, sum of square errors (SSE) was also calculated and listed in Table 5. The SSE results indicate that the adsorption kinetics of MB dye by SPPBC follow the PSO at lowest initial MB concentration (10 mg/L and 50 mg/L). On the other hand, the adsorption kinetics at higher initial MB concentration (100 mg/L, 200 mg/L, and 300 mg/L) follow the PFO kinetics. This observation was reconfirmed by observing the predicted q_e values of PFO model are much closer to the experimental qe values at higher initial MB concentration than the q_e values of PSO model. In fact, the literature reported that the kinetics mainly depends on the initial adsorbate concentration. Moreover, the PSO model is the most preferable model for the lowest initial concentration, while PFO is preferable one for higher initial concentration [40].

6. Isotherm Study

An adsorption isotherm is a plot of equilibrium concentration of an adsorbate on the adsorbent surface versus the concentration of adsorbate in the solution. In this regard, three isotherm models, namely Langmuir [41], Freundlich [42], and Temkin [43], were utilized to study the adsorption isotherm constant and capacities. Langmuir isotherm model indicates a homogeneous adsorption process. Meaning that, the affinity of all adsorption sites towards the adsorbate is equal [44]. In the Freundlich isotherm model the heterogeneity of the surface as well as the exponential distribution of the active sites and the active sites energies are described. Moreover, due to Freundlich model not being restricted to the monolayer formation, it is made possible to apply it to multilayer adsorption [45]. Temkin isotherm model considers the interactions between the adsorbent and the adsorbate in which the extremely large and low concentration values are ignored, hence making this adsorption isotherm model only valid for intermediate concentration ranges [46]. The non-linear formulas of Langmuir, Freundlich, and Temkin are listed by Eqs. (10), (11), and (12) respectively:

$$q_e = \frac{q_{max} K_a C_e}{1+K_a C_e} \quad (10)$$

$$q_e = K_f C_e^{1/n} \quad (11)$$

$$q_e = \frac{RT}{b_T}\ln(K_T C_e) \quad (12)$$

where q_{max} (mg/g) is the maximum adsorption capacity of SPPBC, q_e (mg/g) is the quantity of MB uptake at equilibrium, and n represents the adsorption intensity. K_f (mg/g) $(L/mg)^{1/n}$, K_a (L/mg), K_T (L/mg) are Freundlich, Langmuir, and Temkin constants, respectively. The non-linear isotherm plots of MB dye adsorption are shown in Fig. 7(b), and all the isotherm parameters are listed in Table 6. Based on the R^2 and SSE values, MB dye adsorption was better described by the Langmuir and Temkin isotherm models, which indicates the monolayer and homogeneous distribution onto adsorption sites and preferability at mild concentration levels. The q_{max} value predicted from the Langmuir model was 161.9 mg/g at 49 °C. The efficiency of SPPBC in removing MB dye was compared with other adsorbents as shown in Table 7. SPPBC can be

Table 6. Isotherms parameters of MB adsorption by SPPBC at 49 °C

Model	Parameter	Values
Langmuir	q_{max} (mg/g)	161.9
	K_a (L/mg)	0.29
	R^2	0.97
	SSE	460.8
Freundlich	K_F (mg/g $(L/mg)^{1/n}$)	44.9
	1/n	0.29
	R^2	0.96
	SSE	616.5
Temkin	K_T (L/mg)	24.3
	b_T (J/mol)	101.9
	R^2	0.98
	SSE	420.4

Table 7. Comparative of adsorption capacities for MB by different biochar adsorbents

Biochar adsorbents	q_{max} (mg/g)	References
SPPBC	161.9	This study
Macroalgae and coal-based biochar	353.9	[47]
Orange (Citrus sinensis) peels biochar	208.3	[48]
Date palm fronds biochars	206.61	[49]
Banana pseudostem biochar	146.23	[50]
Fallen leaf-biochar	101.27	[51]
Oak wood biochar	97.55	[52]
Activated reed-derived biochar by tannic acid	77.35	[53]
Date seed biochar	42.57	[54]

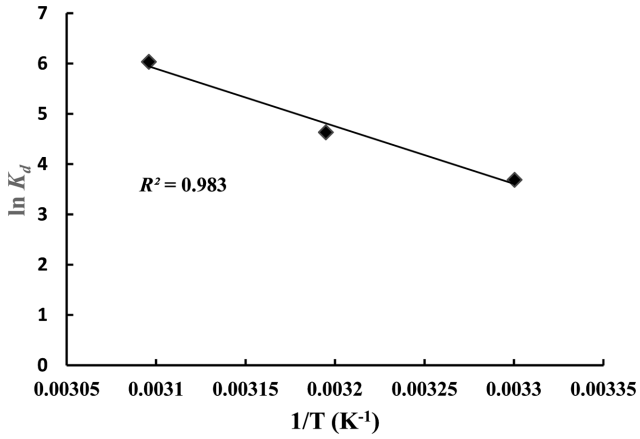

Fig. 8. Van't Hoff plot for MB dye adsorption onto SPPBC (dosage= 0.18 g, pH of solution=9.7, agitation speed=100 strokes and volume of solution=100 mL).

Table 8. Thermodynamic parameters for the adsorption of MB dye by SPPBC

T (K)	k_d	ΔG^o (kJ/mol)	ΔH^o (kJ/mol)	ΔS^o (kJ/molK)
303.15	40.1	−9.3	95.2	0.34
313.15	102.9	−12.1		
323.15	418.2	−16.1		

considered an alternative adsorbent that performed satisfactorily in removing MB dye from aqueous solutions.

7. Thermodynamics Study

Adsorption thermodynamic parameters can be obtained from the van't Hoff plot, which is useful in revealing the adsorption feasibility, spontaneity, and determination of the degree of randomness. The equations related to the Gibbs free energy change (ΔG^o), enthalpy change (ΔH^o), and entropy change (ΔS^o), are presented in

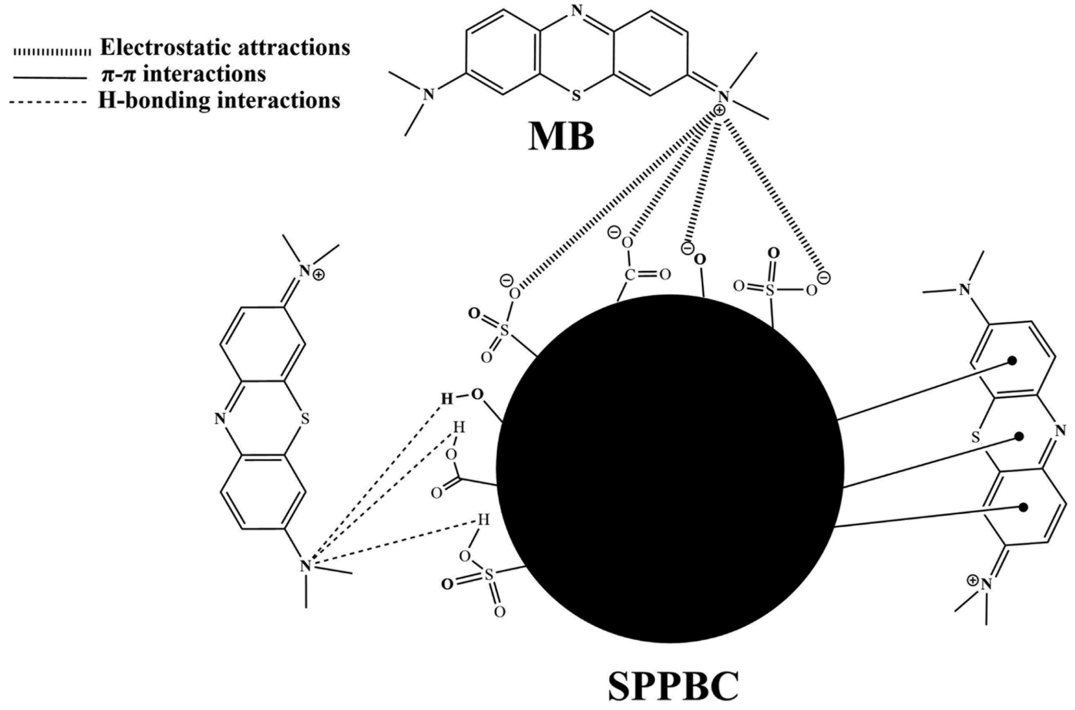

Fig. 9. Illustration of the possible interaction between SPPBC surface and MB dye including electrostatic attraction, hydrogen bonding interactions, and -π interactions.

the following (13)-(16) [55]:

$$\Delta G^o = -RT\ln K_d \quad (13)$$

$$K_d = q_e/C_e \quad (14)$$

$$\Delta G^o = \Delta G^o - T\Delta S^o \quad (15)$$

$$\ln K_d = \left(\frac{\Delta S^o}{R}\right) - \left(\frac{\Delta H^o}{R}\right)\frac{1}{T} \quad (16)$$

The values ΔH^o and ΔS^o were acquired from the plot of ln K_d (K_d: (L/g) is the distribution coefficient for the adsorption) against 1/T (Fig. 8), where the slope and intercept represent ΔH^o, and ΔS^o, respectively. Table 8 shows the negative ΔG^o values, which validated that MB dye adsorption was spontaneous and enhanced at higher temperatures [19]. The positive value of ΔS^o indicated an increased disorder of adsorbate at the solid-liquid interface [55]. The positive value of ΔH^o illustrates that the MB adsorption mode was endothermic [19,55], which is in line with the BBD results that showed an increase in MB removal with increasing temperature.

8. Adsorption Mechanism

The MB dye adsorption mechanisms on the surface of SPPBC could be inferred from the FTIR analysis, which demonstrated the existence of functional groups such as $-O^-$, $-COO^-$, and $-SO_3^-$. Fig. 9 displays various possible interactions that could occur between MB dye molecules and the SPPBC surface. The electrostatic attraction was favored due to the MB dye's cationic nature with the SPPBC negatively charged surface. Another interaction could involve hydrogen bonding between the donor and acceptor groups of the SPPBC-MB system. The π-π interaction also occurred between the π-electron system of the adsorbent surface and the aromatic rings of the MB dye molecules [56]. Similar observation of π-π interaction between the aromatic ring of MB dye molecules and hexagonal skeleton of activated carbon-based martials can be found in literature [19,23,57-59].

CONCLUSION

SPPBC was successfully prepared by thermal activation of PP with H_2SO_4 at 110 °C for 24 h with a fixed impregnation ratio (1 g PP: 1 g H_2SO_4). SPPBC was utilized as a promising adsorbent for removing MB dye using RSM-BBD. The optimized removal conditions were solution pH of 9.7, SPPBC dose of 0.18 g/L, and temperature of 49 °C. SPPBC maximum adsorption capacity for MB dye at equilibrium was found to be 169.1 mg/g. The adsorption mechanisms involved were identified as electrostatic attraction, π-π interaction, and H-bonding. The results illustrated PP biomass waste's feasibility as an inexpensive precursor for preparing SPPBC with satisfactory adsorption ability towards cationic dyes.

ACKNOWLEDGEMENTS

The authors are thankful to the Faculty of Applied Sciences, Universiti Teknologi MARA, Malaysia for facilitating this research work. The authors (Zeid A. ALOthman and Mohammad Rizwan Khan) are grateful to the Deanship of Scientific Research, King Saud University for funding through Vice Deanship of Scientific Research Chairs.

REFERENCES

1. M. Muthukumar, D. Sargunamani, N. Selvakumar and J. V. Rao, *Dyes Pigm.*, **63**, 127 (2004).
2. R. A. Rashid, M. A. M. Ishak and K. M. Hello, *Sci. Lett.*, **12**(1), 77 (2018).
3. Z. Ciğeroğlu, G. Küçükyıldız, A. Haşimoğlu, F. Taktak and N. Açıksöz, *Korean J. Chem. Eng.*, **37**, 1975 (2020).
4. H. A. Rafaie, N. F. M. Yusop, N. F. Azmi, N. S. Abdullah and N. I. T. Ramli, *Sci. Lett.*, **15**(1), 1 (2021).
5. J. Liu, A. Liu, W. Wang, R. Li and W. X. Zhang, *Chemosphere*, **237**, 124470 (2019).
6. S. Shengli, L. Junping, L. Qi, N. Fangru, F. Jia and X. Shulian, *Ecotoxicol. Environ. Saf.*, **165**, 411 (2018).
7. Z. Chu, K. Chen, C. Xiao, D. Ji, H. Ling, M. Li and H. Liu, *J. Taiwan Inst. Chem. Eng.*, **108**, 71 (2020).
8. M. Mourabet, A. El Rhilassi, H. El Boujaady, M. Bennani-Ziatni, R. El Hamri and A. Taitai, *Appl. Surf. Sci.*, **258**, 4402 (2012).
9. S. Wong, N. Ngadi, I. M. Inuwa and O. Hassan, *J. Clean. Prod.*, **175**, 361 (2018).
10. D. A. G. Sumalinog, S. C. Capareda and M. D. G. de Luna, *J. Environ. Manage.*, **210**, 255 (2018).
11. A. Nasrullah, B. Saad, A. H. Bhat, A. S. Khan, M. Danish, M. H. Isa and A. Naeem, *J. Clean. Prod.*, **211**, 1190 (2019).
12. Z. Li, D. Liu, W. Huang, X. Wei and W. Huang, *Sci. Total Environ.*, **721**, 137764 (2020).
13. R. Xiao, J. J. Wang, R. Li, J. Park, Y. Meng, B. Zhou and Z. Zhang, *Chemosphere*, **208**, 408 (2018).
14. S. Rangabhashiyam and P. Balasubramanian, *Ind. Crops Prod.*, **128**, 405 (2019).
15. Y. Xu, Y. Liu, S. Liu, X. Tan, G. Zeng, W. Zeng and B. Zheng, *Environ. Sci. Pollut. Res.*, **23**, 23606 (2016).
16. L. Sun, D. Chen, S. Wan and Z. Yu, *Bioresour. Technol.*, **198**, 300 (2015).
17. X. Xiong, K. M. Iris, S. S. Chen, D. C. Tsang, L. Cao, H. Song and C. S. Poon, *Catal. Today*, **314**, 52 (2018).
18. Y. Xue, B. Gao, Y. Yao, M. Inyang, M. Zhang, A. R. Zimmerman and K. S. Ro, *Chem. Eng. J.*, **200**, 673 (2012).
19. A. H. Jawad, R. Razuan, J. N. Appaturi and L. D. Wilson, *Surf. Interfac.*, **16**, 76 (2019).
20. F. A. Dawodu, O. Ayodele, J. Xin, S. Zhang and D. Yan, *Appl. Energy*, **114**, 819 (2014).
21. S. Lim, C. Y. Yap, Y. L. Pang and K. H. Wong, *J. Hazard. Mater.*, **390**, 121532 (2019).
22. C. Li, Y. Gao, A. Li, L. Zhang, G. Ji, K. Zhu and Y. Zhang, *Environ. Pollut.*, **254**, 113005 (2019).
23. A. H. Jawad, A. S. Abdulhameed and M. S. Mastuli, *J. Taibah Univ. Sci.*, **14**, 305 (2020).
24. H. Li, Q. Deng, H. Chen, X. Cao, J. Zheng, Y. Zhong and S. Deng, *Appl. Catal. A Gen.*, **580**, 178 (2019).
25. Y. Li, F. Wang, Y. Miao, Y. Mai, H. Li, X. Chen and J. Chen, *Bioresour. Technol.*, **307**, 123165 (2020).
26. J. Choi, W. Won and S. C. Capareda, *Ind. Crops Prod.*, **137**, 672 (2019).

27. W. Pongkua, R. Dolphen and P. Thiravetyan, *Chemosphere*, **239**, 124724 (2020).
28. A. Dalvand, R. Nabizadeh, M. R. Ganjali, M. Khoobi, S. Nazmara and A. H. Mahvi, *J. Magn. Magn. Mater.*, **404**, 179 (2016).
29. K. S. Sing, *Pure Appl. Chem.*, **57**, 603 (1985).
30. A. H. Jawad, S. H. Mallah and M. S. Mastuli, *Desalin. Water Treat.*, **124**, 297 (2018).
31. I. Normah and N. A. Nor Aryan Nabila, *Sci. Lett.*, **13**(1), 42 (2019).
32. V. K. Gupta, S. Agarwal, M. Asif, A. Fakhri and N. Sadeghi, *J. Colloid Interface Sci.*, **497**, 193 (2017).
33. N. N. A. Malek, A. H. Jawad, A. S. Abdulhameed, K. Ismail and B. H. Hameed, *Int. J. Biol. Macromol.*, **146**, 530 (2020).
34. A. H. Jawad, A. S. Abdulhameed, N. N. A. Malek and Z. A. ALOthman, *Int. J. Biol. Macromol.*, **164**, 4218 (2020).
35. S. Sheshmani, M. A. Nematzadeh, S. Shokrollahzadeh and A. Ashori, *Int. J. Biol. Macromol.*, **80**, 475 (2015).
36. S. Shengli, L. Junping, L. Qi, N. Fangru, F. Jia and X. Shulian, *Ecotoxicol. Environ. Safe.*, **165**, 411 (2018).
37. A. S. Abdulhameed, A. H. Jawad and A. T. Mohammad, *Bioresour. Technol.*, **293**, 122071 (2019).
38. S. Lagergren, *Vet. Akad. Handl.*, **24**, 1 (1898).
39. Y. S. Ho and G. McKay, *Chem. Eng. J.*, **70**, 115 (1998).
40. S. A. L. Bachmann, T. Calvete and L. A. Féris, *Sci. Environ. Total*, **767**, 144229 (2021).
41. I. Langmuir, *J. Am. Chem. Soc.*, **40**, 1361 (1918).
42. H. M. F. Frenudlich, *J. Phys. Chem.*, **57**, 385 (1906).
43. M. I. Tempkin and V. Pyzhev, *Acta Phys. Chim. USSR*, **12**, 327 (1940).
44. S. Kundu and A. K. Gupta, *Chem. Eng. J.*, **122**, 93 (2006).
45. M. A. Al-Ghouti and D. A. Da'ana, *J. Hazard. Mater.*, **393**, 122383 (2020).
46. H. Shahbeig, N. Bagheri, S. A. Ghorbanian, A. Hallajisani and S. Poorkarimi, *World J. Modell. Simul.*, **9**(4), 243 (2013).
47. T. Fazal, A. Faisal, A. Mushtaq, A. Hafeez, F. Javed, A. A. Din and F. Rehman, *Biomass Convers. Biorefin.* (2019), https://doi.org/10.1007/s13399-019-00555-6.
48. A. H. Jawad, D. T. Al-Heetimi and M. S. Mastuli, *Iran. J. Chem. Chem. Eng.*, **38**, 91 (2019).
49. M. Zubair, N. D. Mu'azu, N. Jarrah, N. I. Blaisi, H. A. Aziz and M. A. Al-Harthi, *Water Air Soil Pollut.*, **231**, 240 (2020).
50. S. Liu, J. Li, S. Xu, M. Wang, Y. Zhang and X. Xue, *Bioresour. Technol.*, **282**, 48 (2019).
51. B. Ji, J. Wang, H. Song and W. Chen, *J. Environ. Chem. Eng.*, **7**, 103036 (2019).
52. A. A. Babaei, S. N. Alavi, M. Akbarifar, K. Ahmadi, A. Ramazanpour Esfahani and B. Kakavandi, *Desalin. Water Treat.*, **57**, 27199 (2016).
53. Y. Wang, Y. Zhang, S. Li, W. Zhong and W. Wei, *J. Mol. Liq.*, **268**, 658 (2018).
54. Z. Mahdi, A. El Hanandeh and Q. Yu, *Waste Biomass Valori.*, **8**, 2061 (2017).
55. R. Ghibate, O. Senhaji and R. Taouil, *Case Stud. Chem. Environ. Eng.*, **3**, 100078 (2021).
56. X. Li, D. Han, M. Zhang, B. Li, Z. Wang, Z. Gong and X. Yang, *Colloids Surf. A Physicochem. Eng. Asp.*, **578**, 123505 (2019).
57. L. Ai, C. Zhang, F. Liao, Y. Wang, M. Li, L. Meng and J. Jiang, *J. Hazard. Mater.*, **198**, 282 (2011).
58. Z. Jia, Z. Li, S. Li, Y. Li and R. Zhu, *J. Mol. Liq.*, **220**, 56 (2016).
59. Z. Zhang and X. Xu, *Chem. Eng. J.*, **256**, 85 (2014).